

Theory of Mott insulator/band insulator heterostructure

Satoshi Okamoto and Andrew J. Millis

Department of Physics, Columbia University, 538 West 120th Street, New York, NY 10027

(Dated: February 2, 2008)

A theory of heterostructures comprised of LaTiO_3 (a Mott insulator) and SrTiO_3 (a band insulator) is presented. The band structure of the Ti d -electrons is treated with a nearest neighbor tight-binding approximation; the electric fields arising from the $\text{La}^{3+}/\text{Sr}^{2+}$ charge difference and the carriers are treated within a Hartree approximation; and the on-site interactions are treated by unrestricted Hartree-Fock. The phase diagram as a function of interaction strength and layer number is determined and predictions are made for optical conductivity experiments. A note worthy finding is that the edges of the heterostructure are generally metallic.

I. INTRODUCTION

“Correlated electron systems” (such as transition metal oxides) are materials in which strong electron-electron or electron-lattice interactions produces behavior incompatible with the standard “density functional plus Migdal-Eliashberg” theory which describes most compounds. The past decade has seen tremendous progress in the physics and materials science of correlated-electron systems. Significant improvements in crystal and film growth, in measurement techniques and in theory have led to a much improved understanding of the bulk properties of these materials. An important finding is that correlated electron systems exhibit a multiplicity of interesting phases (superconducting, magnetic, charge and orbitally ordered) along with associated novel excitations. For recent reviews, see Ref. 1, or the articles in Ref. 2.

The recent success in treating bulk properties suggests that the time is ripe for a systematic study of the surface and interface properties of correlated electron systems. In addition to its basic importance as a fundamental question in materials science, correlated electron surface/interface science should provide the necessary scientific background for study of potential devices exploiting correlated electron properties, because essentially any device must be coupled to the rest of the world via motion of electrons through an interface, and for study of correlated electron nanostructures, because essentially the defining property of a nanostructure is a high surface to volume ratio. The fundamental interest of bulk correlated electron materials lies in the novel phases they exhibit, and we therefore suggest that the fundamental issue for the nascent field of “correlated electron surface science” is “how does the electronic phase at the surface differ from that in the bulk”; in other words, “what is the electronic surface reconstruction.”

This question has begun to attract experimental attention. Hesper and co-workers have shown that the [111] surface of K_3C_{60} differs from bulk because of charge transfer caused by a polar surface.³ Matzdorf and collaborators have demonstrated that in the correlated electron system $\text{Ca}_{0.9}\text{Sr}_{0.1}\text{RuO}_3$ (which exhibits Mott metal-insulator transition), the surface layers remain metal-

lic down to a lower temperature than does the bulk system.⁴ Izumi and co-workers have fabricated “digital heterostructures” composed of different transition metal oxides and have demonstrated changes in electronic phase and other properties depending on the thicknesses of different layers.⁵ In an experimental tour-de-force, Ohtomo, Muller, Grazul, and Hwang have demonstrated the fabrication of atomically precise digital heterostructures involving a controllable number n of planes of LaTiO_3 (a correlated-electron Mott-insulating material) separated by a controllable number m of planes of SrTiO_3 (a more conventional band-insulating material) and have measured both the variation of electron density transverse to the planes and the dc transport properties of the heterostructure.⁶ Their work opens the door to controlled studies both of correlated electron physics in confined dimensions and of the behavior of the interface between a correlated system and a uncorrelated one.

Many physics and material science issues arise in considering the behavior of correlated electrons near surfaces and interfaces. Atomic reconstruction may occur, and may change the underlying electronic structure. For example, the authors of Ref. 4 argue that a change in tilt angle of the surface RuO_6 octahedra increases the electronic hopping, thereby allowing the metallic phase to persist to lower T . Also, as noted e.g. by Hesper and collaborators, a change in structure will lead to changes in Madelung potentials, and to the screening which helps define the values of many-body interaction parameters.³ “Leakage” of charge across an interface may change densities away from the commensurate values required for insulating behavior. Substrate induced strain is well known to change the behavior of films.⁷

Sorting out the different contributions and assessing their effect on the many-body physics is a formidable task, which will require a sustained experimental and theoretical effort. The experiment of Ohtomo *et al.* offers an attractive starting point. In this system, the near lattice match (1.5 % difference in lattice parameter) and chemical similarity of the two components (LaTiO_3 and SrTiO_3) suggests that atomic reconstructions, strain, and renormalizations of many-body parameters are of lesser importance, so the physical effects of electronic reconstruction can be isolated and studied. Further, the near Fermi surface states are derived mainly from the Ti d -

orbitals,⁸ and correspond to narrow bands well described by tight-binding theory. However, the orbital degeneracy characteristic of Ti provides an interesting set of possible ordered phases.

In this paper we undertake a theoretical analysis of the correlated electron behavior to be expected in lattice-matched digital heterostructures of the type created by Ohtomo *et al.*⁶ We focus on electrons in the Ti-derived bands, and include the effects of the long-ranged electric fields arising both from the La atoms and the electronic charge distribution. We treat the extra on-site interactions via a Hartree-Fock interaction. We calculate the electronic phase diagram as a function of on-site interaction parameter and number of La layers and for the relevant phases determine the spatial variation of charge, spin and orbital densities. We obtain a complex set of behaviors depending on interaction strength and number of La layers. Generally, we find a crossover length of approximately three unit cells, so that units of six or more LaTiO₃ layers have a central region which exhibits bulk-like behavior. The outmost ~ 3 layers on each side are however metallic (in contrast to the insulating behavior of bulk LaTiO₃). For very thin superlattices the ordering patterns differ from bulk. We calculate optical conductivity spectra and show that this is a revealing probe of the electronic structure.

The rest of this paper is organized as follows: Section II defines the model, parameter values, and method of study. Section III presents our results for the $T = 0$ phase diagram as a function of interaction strength and number of LaTiO₃ layers. Section IV presents our results for the spatial dependence of the charge density in the small U regime where neither spin nor orbital ordering occur and provides, for this simpler case, an overview of the general features of the electronic structure. Section V studies the onset of spin and orbital order as the interaction and layer thickness are increased. Section VI discusses in more detail the special case 1 layer. Section VII study the interrelation between the metallic behavior and the subband structure, and a stability under parameter variation. Section VIII presents representative results for the optical conductivity, and shows how these may be used to elucidate the electronic structure. Finally, section IX presents a summary of our findings and important future directions, and implications for the general questions of correlated electron surface and interface science, and is designed to be useful to readers uninterested in the details presented in sections II-VIII.

II. FORMALISM

Both LaTiO₃ and SrTiO₃ crystallize in the simple ABO₃ perovskite structure⁹ (more precisely, very small distortions occur which we neglect here) and as noted by Ref. 6 the lattice constants of the two materials are almost identical; $a_{\text{LaTiO}_3} \simeq a_{\text{SrTiO}_3} = 3.9 \text{ \AA}$, minimizing structural discontinuities at the interface and presumably

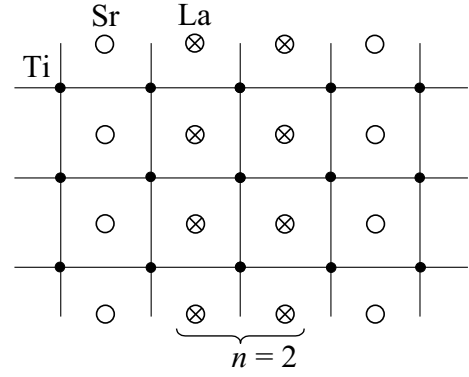


FIG. 1: Schematic figure of the model used in the present study. Open and crossed circles show the positions of Sr and La ions. (La layer number $n = 2$) The dots show the positions of Ti ions. x, y axes are chosen to be parallel to the La plane, and z axis is perpendicular to the plane.

aiding in the growth of high quality digital heterostructures.

In this paper we consider an infinite crystal of SrTiO₃, into which n adjacent [001] planes of LaTiO₃ have been inserted perpendicular to one of the Ti-Ti bond directions, as shown in Fig. 1. We choose the z direction to be perpendicular to the LaTiO₃ planes, so the system has a (discrete) translation symmetry in the xy direction.

The relevant electronic orbitals are derived from the Ti t_{2g} -symmetry d -states, and maybe labeled as d_{xy}, d_{xz}, d_{yz} . The derived bands¹⁰ are to a good approximation given by a nearest neighbor tight binding model with hopping parameter of magnitude $t \simeq 0.3 \text{ eV}$ and spatial structure given by the Slater-Koster formula,¹¹ so the d_{xy} states disperse only in the xy plane *etc.*

We take the electrons to hop between Ti sites according to a nearest neighbor hopping and to feel a potential defined by (i) the Coulomb force arising from the extra charge on the La relative to Sr (ii) the Coulomb force arising from the electrons on other Ti sites and (iii) on-site “Hubbard U and J ” interactions with other electrons on the same site. We take the form of the on-site interactions determined by Mizokawa *et al.*¹² and adopt values as discussed below. Thus

$$H_{\text{tot}} = \sum_a H_{\text{hop}}^{(a)} + \sum_i [H_{\text{Coul}}^{(i)} + H_{\text{on-site}}^{(i)}] \quad (1)$$

with

$$H_{\text{hop}}^{(xy)} = -2t \sum_{\vec{k}\sigma} (\cos k_x + \cos k_y) d_{xy, \vec{k}\sigma}^\dagger d_{xy, \vec{k}\sigma} \quad (2)$$

and similarly for xz, yz . We have

$$H_{\text{Coul}}^{(i)} = V_C(\vec{R}_i) \rho_d(\vec{R}_i) \quad (3)$$

with $\rho_d(\vec{R}_i) = \sum_{a,\sigma} d_{ai\sigma}^\dagger d_{ai\sigma}$ and

$$V_C(\vec{R}_i) = - \sum_{\substack{\text{La sites} \\ j}} \frac{e^2}{\varepsilon |\vec{R}_j^{\text{La}} - \vec{R}_i|} + \frac{1}{2} \sum_{\substack{\text{Ti sites} \\ j \neq i}} \frac{e^2 \rho_d(\vec{R}_j)}{\varepsilon |\vec{R}_j - \vec{R}_i|}. \quad (4)$$

Here the \vec{R}_i are the positions of the $\text{Ti}^{(B)}$ sites in the ABO_3 lattice and \vec{R}_j^{La} label the actual positions of the La ions, which reside on the A sites.

We denote the dielectric function of the host lattice by ε . An interesting issue arises here: SrTiO_3 is a nearly ferroelectric material.¹³ The static dielectric constant becomes very large at long wavelength and low temperatures, but ε is much smaller at high frequencies, room temperature, or short length scales. Also the polarization P will increase more slowly at higher fields, and relevant quantity is P/E . In this paper we have chosen $\varepsilon = 15$ as a compromise between these effects. We discuss the consequences of different choices of ε in the conclusion. We emphasize that incorporating the ferroelectric tendencies of SrTiO_3 (including the associated lattice distortions) in a more realistic manner is an important question for future research.

Finally, the onsite H is

$$\begin{aligned} H_{on-site}^{(i)} = & U \sum_a n_{ai\uparrow} n_{ai\downarrow} + (U' - J) \sum_{a>b,\sigma} n_{ai\sigma} n_{bi\sigma} \\ & + U' \sum_{a \neq b} n_{ai\uparrow} n_{bi\downarrow} + J \sum_{a \neq b} d_{ai\uparrow}^\dagger d_{bi\uparrow} d_{bi\downarrow}^\dagger d_{ai\downarrow} \\ & + J' \sum_{a \neq b} d_{ai\uparrow}^\dagger d_{bi\uparrow} d_{ai\downarrow}^\dagger d_{bi\downarrow}. \end{aligned} \quad (5)$$

The critical issue is the strength of the on-site repulsion. For definiteness we follow other studies which employ the ratios $U' = 7U/9$ and $J = U/9$ which are very close to those determined by Mizokawa.¹² Many workers have used the value $U \sim 5\text{--}6\text{ eV} \sim 18t\text{--}20t$ estimated from high energy spectroscopies.⁸ However, optical conductivity studies of LaTiO_3 and related compounds such as YTiO_3 find rather small gaps, in the range $0.2\text{--}1\text{ eV}$,¹⁴ suggesting $U \sim 2.5\text{ eV} \sim 8t$. In view of this uncertainty we investigate a range U from $\sim 6t\text{--}20t$.

To study the properties of H_{tot} , Eq. (1), we employ the Hartree-Fock approximation replacing terms such as $n_{ai\sigma} n_{bi\sigma}$ by $n_{ai\sigma} \langle n_{bi\sigma} \rangle + \langle n_{ai\sigma} \rangle n_{bi\sigma}$; orbitally off-diagonal expectation values ($\langle d_{ai\sigma}^\dagger d_{bi\sigma} \rangle$) of the type considered by Mizokawa and Mochizuki are stable only in the presence of a GdFeO_3 type distortion which we do not consider. While not exact, the approximation reveals the correct trends and in particular reveals insulating, ordered states in the parameter regimes where these exist. To implement the Hartree-Fock approximation we assume an initial distribution of site, spin and orbital occupancies, obtain the one electron potential by factorizing the interaction terms as described below, compute the band structure, obtain new densities, and iterate until convergence is obtained for some U -values. Many iterations ($\sim 10^3$) are required to obtain well-converged solutions, essentially because of the delicate balance of particle distributions needed to screen the long range part of the Coulomb interaction.

There are two types of solutions to the one-electron equations: bound states, which decay as $|z| \rightarrow \infty$, and

continuum states, which do not. As usual in heterostructure problems the bound states give rise to sub-bands, some of which are partially occupied. The ground state is obtained by filling the lowest sub-bands up to the appropriate chemical potential (determined by charge neutrality); the interaction-related terms in $H_{Coul}^{(i)}$ and $H_{on-site}^{(i)}$ are then recomputed and the procedure is repeated until self-consistency is obtained. Charge neutrality requires that the total density of electrons in the bound-state sub-bands equals the total density of La ions. However, the interplay between electron-La attraction and electron-electron repulsion leads (in almost all of the cases we have studied) to a very weak binding of the highest-lying electron states; indeed for large U the Fermi level of the partially filled sub-bands is only infinitesimally below the bottom of the continuum bands. Also in some regions of the phase diagram, there are several locally stable solutions and it is necessary to compare energies, to determine the ground state. Between 200 and 3000 iterations were required, with the larger number needed either when the Fermi level adjoins the continuum states or when several different states are very close in energy.

We now mention some specific details of our solution to the Hartree-Fock equations. We seek solutions which are bound in the z directions; i.e. functions $\phi(i, xy)$ which decay as layer index $i \rightarrow \pm\infty$, and which depend on the transverse (xy) coordinates as discussed below.

For each orbital α , the functions $\varphi^\alpha(i; xy)$ obey a single particle Schrödinger equation which we write as

$$t_z^{\alpha} a^2 D_{2z}[\varphi^\alpha(i; xy)] + H_{xy}^{(i)} \varphi^\alpha(i; xy) = E \varphi^\alpha(i; xy). \quad (6)$$

Here $D_{2z}\varphi$ is the discretized second order derivative $\varphi_{i+1} - 2\varphi_i + \varphi_{i-1}$ and $t_z^\alpha = t = 0.3\text{ eV}$ for $\alpha = xz, yz$ and $= 0$ for $\alpha = xy$. The term $H_{xy}^{(i)}$ contains the dispersion in the plane of the layers, as well as terms arising from the long-ranges Coulomb interaction [Eq. (3)] and terms arising from the Hartree-Fock approximation. These terms depend on the on-site interactions and on the charge, spin and orbital density in layer i . A general mean-field state would break translation invariance in the xy plane, in a manner whose amplitude would depend on layer index i , thereby mixing the motion in x, y and z directions, leading to a very numerically involved three dimensional self-consistency problem. In order to keep the computations within reasonable bounds and explore wide ranges of parameters, we have in most calculations restricted attention to states which preserve translational invariance in the xy plane. For these states the xy and z motions decouple, and physical quantities may be computed from the solution of a $1d$ problem combined with an integral over a two-dimensional momentum. We also performed some investigations of states with a two-sublattice xy plane structure. In this case, after Fourier transformation on the in-plane coordinate the in-plane Hamiltonian may be written

$$H_{xy}^{(i)} = \begin{pmatrix} V_i + \Delta^i & \varepsilon_p \\ \varepsilon_p & V_i - \Delta^i \end{pmatrix} \quad (7)$$

with V_i the part of the potential which is independent of sublattice, Δ^i the part which alternates between sublattices and ε_p the in-plane dispersion in the reduced Brillouin zone. The variation of the mixing term Δ^i with layer requires a separate treatment, lengthening the numerical analysis considerably.

III. PHASE DIAGRAM

In this section we present and discuss the calculated phase diagram. The geometry of the heterostructure distinguishes between the xy orbital and the $\{xz, yz\}$ orbitals. As noted above, we assume translation invariance in the xy plane. The symmetries which may be broken are therefore spin rotation and orbital rotation (xz and yz) and inversion along with translation invariance in the xy plane. Also, although it does not have precise meaning except in the $n \rightarrow \infty$ limit, it is physically sensible to interpret results in terms of z -direction translation symmetry breaking when the spin or orbital density oscillates with respect to the total charge density.

Our calculated phase diagram is shown in Fig. 2. For reasons of computational convenience in scanning a wide range of parameters, we considered mainly phases with translation invariance in the xy plane, however for $n = \infty$ and $n = 1$ we considered also an xy -plane two sublattice symmetry breaking. We found in agreement with previous calculations^{12,15,16,17} that the fully staggered phase is favored at $n = \infty$, but xy -plane symmetry broken states could not be stabilized in the one layer case. We have not yet studied more general symmetry breakings for intermediate layer numbers, but physical arguments presented below strongly suggest that these phases only occur for larger numbers of layers ($n \gtrsim 6$).

Four phases are found: a small U phase with no broken symmetry, and intermediate U phase with in-plane translation-invariance spin order, but no orbital order, and a large U phase with both spin and orbital order. The lower U transition line varies smoothly with layer number, while the larger U transition is essentially independent of layer number for $n > 1$. Further, the $n = 1$ intermediate U phase is ferromagnetic whereas for $n > 1$ the intermediate U phase is antiferromagnetic. As will be shown in sections below this behavior can be related to the sub-band structure but the essential reason is that for small n the charge density is spread in the z direction, so no layer has a density near 1.

For all n , the lower- U transition is found to be second order. As U is increased above this value, the magnetization increases rapidly and the upper transition is strongly first order. Fig. 3 shows an example of the procedure used to determine the location of the phase boundary and the order of the transition. The upper panel of figure 3 displays the energies of several different phases. We identify U_{c1} as the point where the different energies converge (this is most easily done from a plot, not shown, of the energy differences on an expanded scale) and U_{c2} from

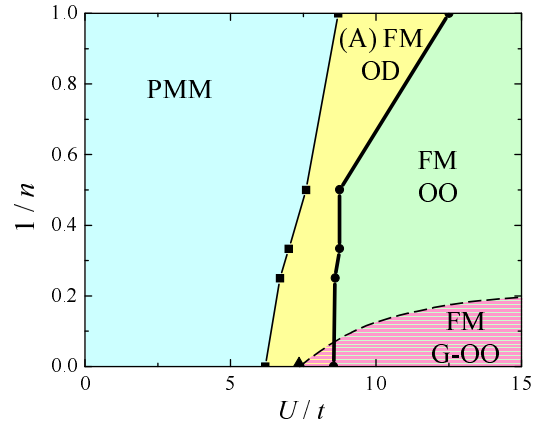


FIG. 2: Theoretical ground state phase diagram as a function of the on-site Coulomb interaction U and inverse of the La layer number n . Parameter values are chosen to be $U' = 7U/9$ and $J = U/9$. $e^2/(\varepsilon at) = 0.8$ which corresponds to $\varepsilon \sim 15$ with a lattice constant $a = 3.9 \text{ \AA}$ and transfer intensity $t = 0.3 \text{ eV}$. The triangle is the critical U to the (π, π, π) orbital ordering at $n = \infty$ case. The broken line shows the expected phase transition to the (π, π, π) antiferromagnetic c

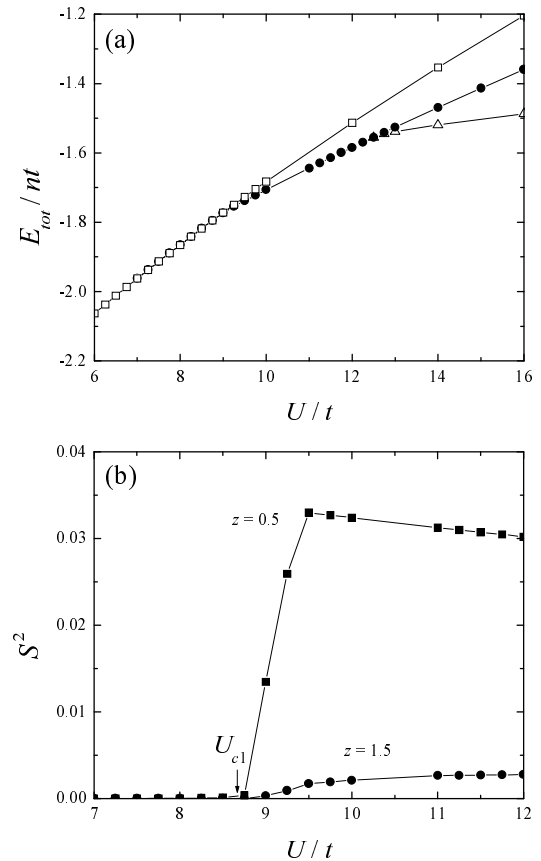


FIG. 3: (a) Energy as a function of U ($n = 1$). Open squares: the spin and orbital-disordered state, filled squares: the spin-order orbital-disorder state, open circles: the spin and orbital-ordered state. (b) Square of magnetization as a function of U in the intermediate coupling region ($n = 1$).

the lowest crossing point of the energy curves. That the energies of two qualitatively different phase states cross at U_{c2} identifies this as a first order phase transition, that the energies merge at U_{c1} suggests a second order transition. Further evidence is provided by panel (b), which shows, on an expanded scale, the magnetization as a function of $U - U_{c1}$, and suggests a continuous decrease to zero.

The comparison to the $n = \infty$ limit is subtle. In bulk LaTiO_3 exhibits a (π, π, π) type antiferromagnetic ordering. Theoretical calculations (apparently confirmed by very recent NMR experiment, and x-ray and neutron diffraction experiments)^{18,19} suggest a four sublattice structure which is very close to a $(0, 0, \pi)$ -type orbital ordering²⁰ differing slightly from the $(0, 0, \pi)$ ordering studied here. Stabilizing the observed state apparently requires a lattice distortion not included in the model studied here. As U is increased from zero the $n \rightarrow \infty$ limit of the model considered here has a phase transition which we believe to be of second order to an incommensurate antiferromagnetic state with a wave vector which is an extremal spanning vector of the Fermi surfaces of the bands arising from two of the orbitals (say xz, yz) and which turns out to be very close to $(0, 0, \pi)$. (In fact, for reasons of numerical simplicity we studied $(0, 0, \pi)$ ordering and found a very weakly first order transition.) This transition is followed by a strongly first order transition to one of a degenerate manifold of states characterized by ferromagnetic spin order and (π, π, π) orbital order. To maintain continuity with the heterostructure calculations we have also suppressed the (π, π, π) ordering and located the phase boundary to the (metastable) $(0, 0, \pi)$ -orbital spin-ferromagnetic state. We believe the (π, π, π) -orbital spin-ferro state we have found is a reasonable surrogate for the actual Mochizuki-Imada state found in experiment. Although this state is favored at $n \rightarrow \infty$, the physical origin, explained below in more detail, of our inability to stabilize states with broken in-plane translation invariance at $n = 1$ suggests that the (π, π, π) phases only occur for rather thick superlattices. The essential point is that, for $n < 6$, the solution in the large U limit consists of several partially filled sub-bands, which have effectively minimized their interaction energy but which gain considerable kinetic energy from motion in the xy plane. Breaking of xy translation symmetry would reduce this kinetic energy gain without much decreasing the already saturated interaction energy while z -direction kinetic energy is quenched by the confining potential.

The estimate of $U = 8t$ - $10t$ derived from optical measurements on bulk, and from the recent work on the nature of the ordered phase suggests an interesting series of phase transitions may occur as layer thickness is varied.

IV. SMALL U REGION

In this section we present and discuss the results obtained for $U < U_{c1}$ where no symmetry breaking is

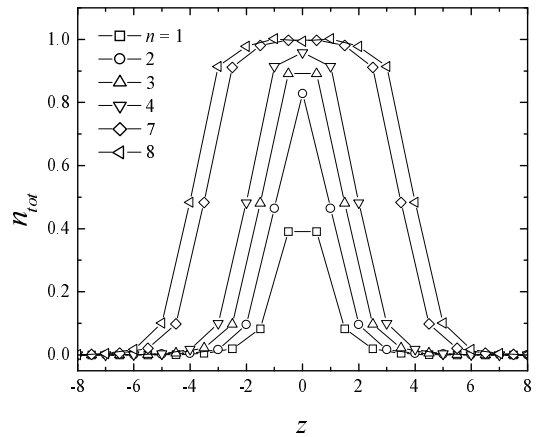


FIG. 4: Calculated total electron density in the small U region ($U = 6t$). Our results (not shown) for larger U values are almost identical.

observed. Although the system geometry implies xy and $\{xz, yz\}$ orbitals are inequivalent, the occupancies of those orbitals are found to be almost the same; the ratio at the center site is given by $(n_{xz} - n_{xy})/n_{xz} = 0.023, 0.098$ and 0.049 for $n = 1, 2$ and 3 , respectively, at $U = 6t$. Therefore, we mainly focus on the spatial distribution of the total electron density below.

Numerical results for the electron density for several choices of La layer n and $U = 6t$ are shown in Fig. 4. Here we set the origin of z axis at the center of n La layers. Electron density is symmetrically distributed around $z = 0$. The density at the center site rapidly increases with increasing n , and exceeds 0.9 at $n = 6$. However, for this and larger U values, the charge density never exceeds unity, even at the center sites. Fig. 4 shows clearly that for thick layers the length scale over which density vary is about three unit cells, and this number is almost independent of n , and depends somewhat on ε and weakly on U .²¹ Thus, at least 6 layers seem to be required before bulk behavior is recovered in the central region. As is well known, SrTiO_3 is close to ferroelectric, and the long wave-length, and linear response dielectric constant becomes about 20000 at the lowest temperature.¹³ The present results involve ε at short scales, and are clearly outside the linear response regime. However, temperature dependent changes in the density profile should occur and are worth experimental study. Another interesting feature to note is that for all ε and U studied the electron and hole distributions at large n are almost symmetric at the edge $z = n/2$; $n_{tot}(z)$ and $1 - n_{tot}(n/2 - z)$ fall on almost the same line (not shown).

It might be interesting to compare the present numerical results ($n = 1, 2$) with the experimentally observed Ti^{3+} spatial distributions.⁶ The observed Ti^{3+} decay length of Ti^{3+} is about 2 nm (5 unit cells) in both $n = 1$ and 2, which is longer than the present theoretical results (about 3 unit cells). The reported La-ion distribution suggests that the spatial resolution of the

EELS measurement is about 0.4 nm (1 unit cell). Inclusion of such effect makes the density distribution profiles closer to the experimental ones, but the experimental distributions are still broader than the present theoretical ones. One possibility is La/Sr interdiffusion (not considered here). An alternate origin could be a chemical shift of the Ti t_{2g} level. Here we have considered only the long-range Coulomb energy, but an additional contribution arising from the slightly different local structure [small ionic radius of La^{3+} (1.045 Å) than that of Sr^{4+} (1.13 Å)]²² could bring the La-Ti d -levels closer to Sr-Ti d -levels. This effect has not been included in this study.

V. ONSET OF POLARIZATION; LARGER U

This section presents results for large U values, where spin and orbital orderings are observed. The main focus is on how the orderings are developed.

Figure 5 (a) and (b) show the electron densities per orbital in the intermediate coupling regime ($U = 8t$) with $n = 2$ where only spin ordering is observed. The difference between the $\{xz, yz\}$ and xy occupancy arise only from the symmetry. As a comparison, electron densities per orbital and spin in the metastable paramagnetic state are also shown (crossed squares). From the difference between the up and down electron occupancy, one can notice that the spin density oscillates around the center site. (although no site is fully polarized) In contrast for $n = 1$ and $8t < U < 12t$, the magnetic state is different: the spins align ferromagnetically. The behavior at $n = 1$ can be attributed to the lower charge density at each site implying low occupancy of each sub-band, so a small shift between the up and down electron sub-bands can stabilize the fully polarized state. On the contrary, ferromagnetic spin ordering at $n \geq 2$ comes from a delicate balance between the confinement potential and on-site Coulomb repulsion.

The electron densities per spin and orbital in the strong coupling regime ($U = 10t$) are shown in Fig. 5 (c) and (d). The difference between xz and yz orbital occupancy clearly indicates antiferro-type orbital ordering along the z direction $(0, 0, \pi)$. One can also notice that spin polarization is almost complete. A tiny amount (less than 1 %) of down spin electrons exist only in the xy orbitals. Note that the orbital ordering in the strong coupling regime is different from that expected in the bulk limit where translational symmetry in xy plane would also be broken. In the small n region, the symmetry in xy is expected to be conserved because this symmetry is favorable to gain the kinetic energy by two dimensional electron motion.

VI. $n = 1$, POSSIBILITY OF STAGGERED IN-PLANE ORDERING

In this section, we discuss special features of the $n = 1$ case. Within the Hartree-Fock approximation we have

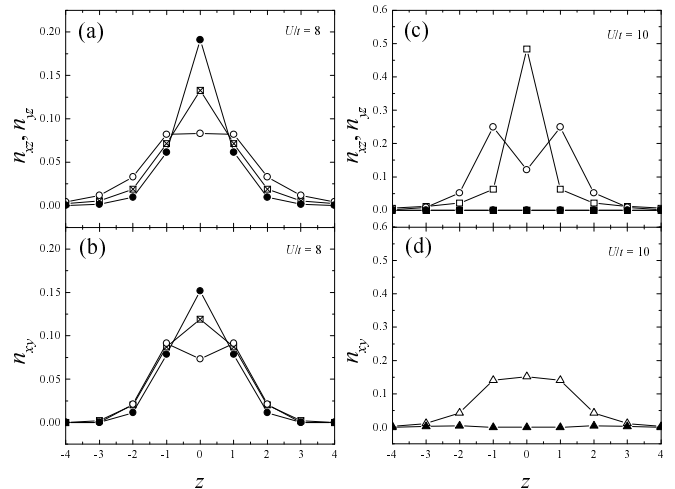


FIG. 5: Electron density per spin and orbital in the intermediate coupling regime $U = 8t$ (a,b) and the strong coupling regime $U = 10t$ (c,d) for a heterostructure with two La layers ($n = 2$). Open and filled symbols show the densities of the up and down spin electrons, respectively. Circles and squares in (a,c) are for the xz and yz , respectively. Crossed squares in (a,b) show the electron density per spin and orbital in a metastable paramagnetic state.

not found any stable states which break xy plane translational invariance. We see from Fig. 4 that at essentially all U the occupancy of any particular orbital state is low. For $U \gtrsim 13t$ the orbital ordering in the z direction (say xy occupancy to the left of the La layer and yz occupancy to the right), along with the ferromagnetism effectively eliminates the on-site interaction contribution to the Hartree-Fock energy, while the fact that the one electron is shared between the two bands means that at each sub-band there is a large kinetic energy gain of order $-\frac{2t}{\pi} \sin p_F$ per sub-band. We believe this physics explains why we at $n = 1$ have been unable to stabilize a state with two-sublattice in-plane symmetry breaking. In bulk at large U , the kinetic energy is quenched and the (π, π, π) state is stabilized relative to the $(0, 0, \pi)$ state by a superexchange of approximately $2t^2/(U' - J) \sim 3t^2/U$ but in the $n = 1$ superlattice the band energy gain is approximately $-\frac{2t}{\pi} \sin p_F$. Indeed this argument suggests that until the band filling becomes close to 1 (which only happens for $n \gtrsim 6$) the kinetic energy gain in xy -invariant states is larger than the superexchange energy gained by ordering so that for a range of small n (perhaps $n < 6$) staggered in-plane ordering may be neglected.

We do expect the xy -translation invariant states we have found to be unstable to some form of weak incommensurate density wave ordering, because the resulting sub-band structure has a one-dimensional character from the xz and yz sub-bands. However, this ordering is expected to be weak because the residual interactions, not already included in our Hartree-Fock solution, are not strong. For example, in the $U > 13t$ regime, the on-site interactions are fully quenched by

the ferromagnetic ordering so incommensurate charge density wave is driven only by the $2p_F$ component of the long ranged Coulomb interaction, which we estimate from the sub-band charge distribution with half width ξ to be $V_c(2p_F) \approx C (2e^2/\epsilon a)$ with $C = \int_0^\infty du \exp[-u^2(\pi\xi/a)^2]/\sqrt{1+u^2} \approx 0.3-0.4$. For the parameters used here $V_c\chi_{2p_F} \sim \lambda \ln(E_F/T)$ with $\lambda \ll 0.1$, so the instability occurs at a very low T . We note, however, that the precise critical behavior of the second order small U transition found in our Hartree-Fock approximation is likely to be complicated by the additional effects of $2p_F$ instabilities in the quasi one dimensional bands. We leave this interesting issue for future research.

VII. METALLIC EDGE AND STABILITY UNDER PARAMETER VARIATION

The experimental results of Ohtomo *et al.*⁶ show that the interface between the two types of insulators supports a metallic state. From numerical results for thick layer (Fig. 4), one finds a central region where $n \simeq 1$, in which one expects bulk-like behavior, and an edge region with $n \ll 1$, which one might expect to exhibit metallic behavior. In this section, we study the interrelation between the subband structure and metallic behavior. We show that the edge region is responsible for the metallic behavior, and study the dependence of the metallic behavior on parameter changes.

Within the Hartree-Fock method we use here, physics of the metallic edge is manifested as follows. There are many bound-state solutions (wave functions decaying as $|z|$ is increased away from the heterostructure), whose dispersion in the in-plane direction gives rise to sub-bands. For thin heterostructures, all sub-bands are partially filled (implying metallic behavior in the heterostructure plane) whereas for thick heterostructures (in ordered phases), some sub-bands are fully filled and some are partly filled. The fully filled sub-bands have z -direction wave functions implying charge density concentrated in the middle of the heterostructure, whereas the partially filled bands have charge concentrated near the edges. The upper panel of Fig. 6 shows the density profiles and the occupancy of partially filled bands for the heterostructure with $n = 6$ and $U/t = 10$ in an orbitally ordered ferromagnetic phase. We observe partially filled bands corresponding to metallic behavior at the heterostructure edges where the density drops from ~ 1 to ~ 0 .

Two key assumptions underlying the calculations presented so far are the translation invariance of the on-site energy ϵ_0 (because in both components of the heterostructure the electronically active ion is octahedrally coordinated Ti) and relatively large value for the dielectric constant (to represent the nearly ferroelectric nature of $SrTiO_3$). We investigate the sensitivity of this result to changes in these parameters. The lower panel of Fig. 6 shows the changes in the density profile and in the oc-

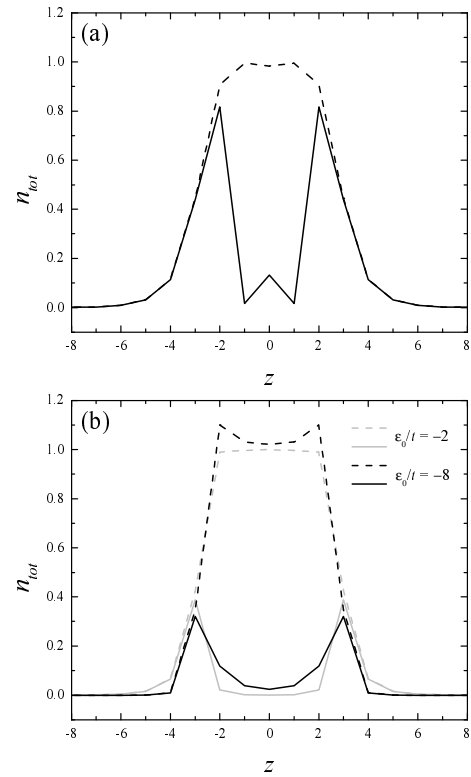


FIG. 6: *Upper panel:* density profile (dashed line) and density in partially occupied bands of heterostructure with $n = 6$, $U/t = 10$ and $\epsilon = 15$ calculated in orbitally-ordered ferromagnetic phase. *Lower panel:* Density profile (dashed lines) and density in unoccupied bands (light and heavy solid lines) for on-site binding to Ti sites in heterostructure (on site energy for Ti) between two La planes ϵ_0 ; on site energy for "edge" Ti sites (between Sr and La planes) $\epsilon_0/2$.

cupancy of partially filled bands occurring if the on-site energy is changed for sites near La sites. Here, we have chosen the site energy of those Ti sites which sit between two Sr planes to be zero, the energy of a Ti site between two La planes to be $\epsilon_0 < 0$ and the energy of a Ti site between a La plane and a Sr plane to be $\epsilon_0/2$. For $\epsilon_0 = 0$ several partially filled bands exist, leading to a high density of metallic electrons. As ϵ_0 is decreased, the electronic structure rapidly rearranges so that most bands become fully filled. However, even for the largest ϵ_0 the geometry ensures that one electron always remains to be shared between two nearly degenerate bands, one on either side of the heterostructure, so the metallic behavior remains robust.

We may similarly consider changes occurring as the dielectric constant is varied. Fig. 7 shows the paramagnetic phase density profile occurring as the dielectric constant is varied over a wide range. The main effect is to decrease the tailing of charge density far into the $SrTiO_3$ layer. However, there again remains one electron to be shared between the two edge subbands, the basic phenomenon of partly filled bands at the edge is unaffected.

Summarizing, for reasonable parameters we find that

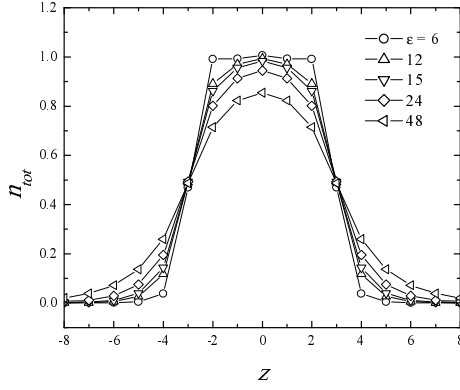


FIG. 7: Dependence of total charge density on dielectric constant calculated for paramagnetic phase of 6 layer heterostructure with $U/t = 10$ in paramagnetic phase.

there are always partially filled bands, corresponding to metallic behavior at the heterostructure edges. The possibility of metallic behavior at the edge of a Mott insulator system appears to be confirmed by the experimental results of Ohtomo *et al.*⁶ would be interesting study further both experimentally and by more sophisticated theoretical methods.

VIII. OPTICAL CONDUCTIVITY

There are two classes of solutions to the Hartree-Fock equations: bound states, which have wave functions which decay as $|z|$ is increased away from the La layers, and continuum states, extended in all three directions. Although the existence of sharply defined single-particle states at all energies is an artifact of the Hartree-Fock approximation, we expect this qualitative structure to survive in a more sophisticated treatment. Therefore, in this section we use the Hartree-Fock approximation to show how optical conductivity can provide information on the nature and filling of the bound states. We also present a qualitative discussion of the effect of interactions beyond Hartree-Fock.

We consider electric field directed perpendicular to the La-planes (parallel to z) and use the Peierls-phase approximation to determine the current operator

$$\hat{J}_z = -it \sum_{ia=xz,yz} [d_{ai\sigma}^\dagger d_{ai+\hat{z}\sigma} - h.c.]. \quad (8)$$

We then evaluate the usual Kubo formula using the Hartree-Fock eigenstates. Note that in the nearest neighbor tight binding approximation the d_{xy} states do not couple to z -electric field, so we will not discuss them in this section.

Figure. 8 shows the calculated $T = 0$ conductivity for the case of one La layer, and two values of U : $U = 6t$ (light curve), for which the system is in the spin and orbital disordered phase, and $U = 10t$ (heavy curve),

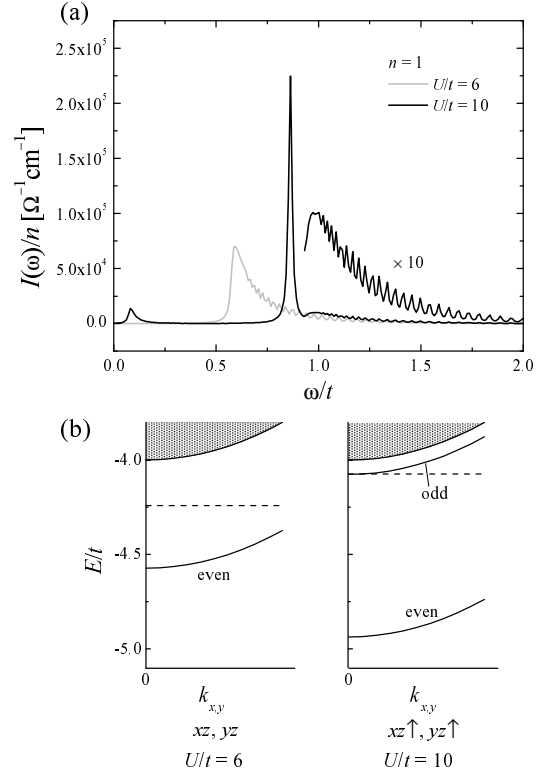


FIG. 8: (a) Optical conductivity for $n = 1$ with $U = 6t$ (small U regime) and $10t$ (intermediate U ferromagnetic state). Electric field E is chosen to be parallel to z . Delta functions are approximated as Lorentzian with the half-maximum half-width $0.1t$. (b) Schematic illustrations of sub-band energy structure at $U = 6t$ (left) and $U = 10t$ (right). Shaded areas show the continuum state. Broken lines show the Fermi energy.

for which the system is in the ferromagnetic, orbitally disordered state.

For $U = 6t$ the xz, yz part of the spectrum (shown in the lower left panel) consists of one four-fold degenerate bound-state sub-band, containing approximately $1/6$ electron per spin per orbital, as well as empty continuum bands. The optical spectrum therefore consists of one feature, corresponding to a bound-continuum state transition. The absorption is peaked at the bound state energy, the width reflects the degree of overlap between continuum and bound state energies. The oscillator strength is related to the kinetic energy in the z direction, and is approximately $10^4 \Omega^{-1} \text{cm}^{-1}/\text{La}$. We expect this spectrum to be very little affected by correlation effects beyond Hartree-Fock, because the basic bound state energetics are fixed by charge neutrality and Coulomb interaction, and the final states are continuum states, which are delocalized in space.

Also shown in the upper panel of Fig. 8 is the spectrum corresponding to $n = 1$ and $U = 10t$. For these parameters the electronic structure has changed (lower right panel of Fig. 8); there are now two sub-bands; one more strongly bound than in the $U = 6t$ case and holding

more electrons (but still only approximately 1/3 filled) and one only very slightly filled band. The calculated $\sigma(\omega)$ correspondingly exhibits three features, a weak low energy ($\omega \sim 0.1t$) feature arising from transitions from the very slightly filled bound to the continuum, a sharp higher energy ($\omega \sim 0.9t$) feature arising from the intersubband transition (allowed because the lower sub-band is even under $z \leftrightarrow -z$ and the upper is odd) and a very broad feature from lower bound-continuum transitions. The intersubband transition contains about 2/3 of the total oscillator strength; the remainder is mainly in the bound-state to continuum peak. We note that as expected on general grounds, the presence of a bound-state to bound-state transition sharply reduces the weight in the continuum (compare $U = 8t, 10t$), essentially because of the requirement that the continuum states be orthogonal to both bound states.

Within the model we have used the intersubband transition is a delta function, because lifetime effects have been neglected and the x, y and z direction dispersions decouple, so the 2 sub-bands disperse in the same way as k_x or k_y is varied. The dispersions decouple because we have adopted a nearest neighbor tight binding model, however this is believed to be reasonably accurate in practice. A potentially more significant source of broadening is the ‘‘Hubbard U ’’ interaction. Experience from simpler models suggests that for these U -values (of order of the critical value for the bulk system Mott transition) and electron concentration (less than 0.4 electrons per layer, far from the Mott value $n = 1$) these effects are not too severe: essentially because the probability of 2 particle collisions scales as n^2 , only a small fraction of the spectral weight will be shifted to an ‘‘upper Hubbard band’’ feature at an energy $\sim U$, and lifetime broadening will be rather less than the Fermi energy, so roughly we expect the peak to remain unchanged. These arguments apply also to the other cases we consider below.

We now discuss the $n = 2$ case. In the small U paramagnetic, orbital disordered case, the electronic spectrum exhibits two bound-state sub-bands; arising from a more strongly bound even parity state and a weakly bound odd parity state. The band structure is very similar to that shown in the right panel of Fig. 8 (b), but without spin polarization. The optical conductivity (not shown) is essentially the same as the $U = 10t$ curve shown in Fig. 8. Increasing U to $U = 8t$ leads to a spin ordered (here ferrimagnetic) orbitally disordered state, with four sub-bands [three below μ and partially occupied] and correspondingly two bound-state to bound-state transitions (one for each spin) and three bound-state to continuum transitions (the middle one of which is evidently extremely weak).

As a final example, we show the optical spectrum and energetics for the spin-ferro orbital-antiferro $U = 10t$ state. Five bound states now occur, and correspondingly three sharp peaks (recall the optical selection rule allows coupling only from even to odd parity states). Four bound-state-continuum transition should be visible (the

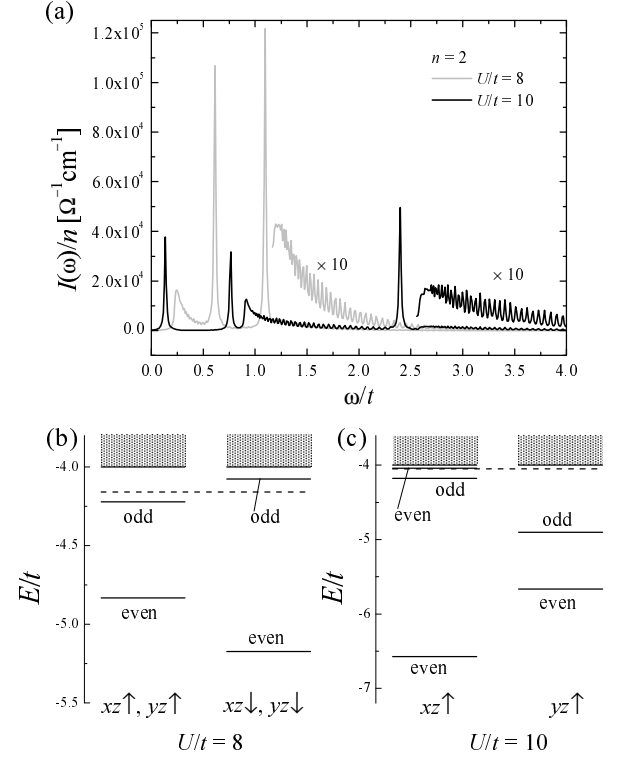


FIG. 9: Optical conductivity for $n = 2$ with $U = 8t$ (intermediate U ferrimagnetic state) and $10t$ (large U ferromagnetic orbital ordered state). Schematic illustrations of sub-band energy structure at $U = 8t$ (b) and $U = 10t$ (c). Shaded areas show the continuum state. Broken lines are the Fermi energy. Remark: band curvature not shown.

highest-lying xz even parity state is essentially unoccupied) but again all are weak and the lowest-lying (arising from the odd d_{xz} band) is especially weak because the low-lying even-parity continuum states must be orthogonal to the even-parity bound state, which absorbs all the oscillator strength.

To summarize: the electronic spectrum consists of a number of different sub-bands (with the detailed structure depending on number of La layers and on the nature of the ordering, if any). The optical spectrum for z -polarized light is predicted to consist of relatively sharp peaks, which may be assigned to the different optically allowed intersubband transitions, along with broad features (often rather weak) associated with transitions from sub-bands to the continuum.

IX. SUMMARY AND CONCLUSION

In this paper we studied theoretically the phase diagram and electronic properties of a ‘‘correlated heterostructure’’ model involving n layers of a material which in bulk is a Mott insulator, embedded in an infinite band insulator. The specific features of the model we study were chosen to reproduce the $\text{LaTiO}_3/\text{SrTiO}_3$

superlattice system studied by Ohtomo *et al.*, but we hope that our results will shed light also on the more general question of the physics of the interface between a strongly correlated and weakly correlated systems.

A crucial feature of the experimental $\text{LaTiO}_3/\text{SrTiO}_3$ system studied by Ohtomo *et al.* is the almost perfect lattice match between the two systems. These authors argued that this implies that the only difference between the Mott insulating and band insulating regions arises from the different charge of the $\text{La}(3+)$ and $\text{Sr}(2+)$; in particular the crystal structure and atomic positions are expected to remain relatively constant throughout the heterostructure. Of course, the asymmetry present at the $\text{LaTiO}_3/\text{SrTiO}_3$ interface must induce some changes in atomic positions: a TiO_6 octahedron is negatively charged, and so if it sits between a Sr plane and a La plane it will be attracted to the latter, and also distorted, because the positively charged Ti will tend to move in the opposite direction. The experimentally determined Ti-Ti distances shown in Fig. 1 of Ref. 6, along with the distortion in that paper, suggests that the changes in Ti-Ti distance are negligible. In this circumstance, changes in O position along the Ti-O-Ti bond change hoppings only in second order. We therefore neglected these effects and assumed that the electronic hoppings and interaction parameters remain invariant across the heterostructure. However, we emphasize that properly accounting for the effect of atomic rearrangements inevitably present at surface and interface is crucial. We further note that lattice distortions appear to be important in stabilizing the observed bulk state, but may be pinned in a heterostructure. Extending our results to include these effects is an important open problem.

In the calculation reported here the heterostructure is defined only by the difference (+3 vs +2) of the La and Sr charge. The calculated electronic charge density is found to be controlled mainly by electrostatic effects (ionic potentials screened by the electronic charge distribution). Results, such as shown in Fig. 4 for $U = 6t$, are representative of results obtained for a wide range of on-site interaction U . We find generally that significant leakage of charge into the band insulator region occurs. The width of the transition region must depend on the relative strength of the z -direction hoppings and the confining potential. For the parameters studied here, the transition region is about 3 layers (so one needs about 7 La layers to obtain a central region with bulk behavior), and that the $n = 1$ case is special because the La counterions sit between the Ti planes. We note, however, that the moderate to large U -values which we study do ensure that even for thick superlattices the charge density on the central layers never becomes greater than unity.

The calculated width is found to be somewhat less than that found by Ohtomo *et al.*, broadening our distribution by the experimental uncertainty (obtained from the La positions) leads to calculated width about 2/3 of mea-

sured ones. Whether the difference arises because we have overestimated the confining potential or for some other reason such as La/Sr interdiffusion remains to be determined.

We now turn to our calculated phase diagram shown in Fig. 2. It is expected on general grounds that decreasing the number of La layers will raise the interaction values required for obtaining ordered states. Further, the specific structure of the system of present interest implies an odd-even alternation. Both of these features are indeed observed in our calculation. Our calculation, in combination with the U -values inferred from optics, suggests that the La/SrTiO_3 system may be in the interesting ($U \sim 7t$ - $12t$) parameter regime in which one or more phase boundaries may be crossed by varying La layer number. A further point, perhaps especially relevant to systems such as titanates which allow for orbital ordering and orbitally dependent hopping, is that the structural anisotropy intrinsic to the heterostructure may favor different ordering patterns than those found in bulk. Thus we find for the thinnest heterostructures different phases with more translational invariance than found in bulk. We note, however, that in the Ti case the “edge states” have a quasi one-dimensional character with an incommensurate filling, perhaps favoring incommensurate charge, spin or orbital ordering at the edge.

The issue of the transport properties of the heterostructure is an important open question, especially in light of the interesting transport data of Ref. 6. A crucial experimental finding is that metallic conduction is always observed, consistent with our prediction of conducting edge states. However, we do not have a qualitative understanding of the Hall data, because within the Hartree-Fock approximation the Hall resistivity is obtained by adding up the contributions of the different sub-bands. The contributions to σ_{xy} arising from the quasi one-dimensional xz, yz sub-bands are controlled by weak deviations from the nearest neighbor hopping approximations, which control the mixing between the two bands and the reconstruction of the Fermi surface of the crossing point. It is difficult to make general statements without more detailed band structure information, but some degree of compensation is expected.

Other important issues for future research include study of correlation effects beyond the Hartree-Fock approximation, inclusion of the coupling between atomic rearrangements, orbital ordering and electronic hopping parameters, and more sophisticated treatment of the dielectric properties of SrTiO_3 .

Acknowledgements We acknowledge very helpful conversations with H. Hwang and M. Potthoff. This research was supported by NSF DMR-0338376 (A.J.M.) and JSPS (S.O.).

-
- ¹ M. Imada, A. Fujimori, and Y. Tokura, *Rev. Mod. Phys.* **70**, 1039 (1998).
 - ² Y. Tokura and N. Nagaosa, *Science* **288** 462 (2000).
 - ³ R. Hesper, L. H. Tjeng, A. Heeres, and G. A. Sawatzky, *Phys. Rev. B* **62**, 16046 (2000).
 - ⁴ R. Matzdorf, Z. Fang, Ismail, J. Zhang, T. Kimura, Y. Tokura, K. Terakura, and E. W. Plummer, *Science* **289**, 746 (2000).
 - ⁵ M. Izumi, Y. Murakami, Y. Konishi, T. Manako, M. Kawasaki, and Y. Tokura, *Phys. Rev. B* **60**, 1211 (1999).
 - ⁶ A. Ohtomo, D. A. Muller, J. L. Grazul, and H. Y. Hwang, *Nature* **419**, 378 (2002).
 - ⁷ M. Izumi, Y. Ogimoto, Y. Konishi, T. Manako, M. Kawasaki, Y. Tokura, *Mat. Sci. Eng. B* **84**, 53 (2001); A. Biswas, M. Rajeswari, R. C. Srivastava, Y. H. Li, T. Venkatesan, R. L. Greene, and A. J. Millis, *Phys. Rev. B* **61**, 9665 (2000); A. Biswas, M. Rajeswari, R. C. Srivastava, T. Venkatesan, R. L. Greene, Q. Lu, A. L. de Lozanne, and A. J. Millis, *Phys. Rev. B* **63**, 184424 (2001).
 - ⁸ T. Saitoh, A. E. Bocquet, T. Mizokawa, and A. Fujimori, *Phys. Rev. B* **52**, 7934 (1995).
 - ⁹ D. A. Maclean, H.-N. Ng and J. E. Greedan, *J. Solid State Chem.* **30**, 35 (1979).
 - ¹⁰ H. Fujitani and S. Asano, *Phys. Rev. B* **51**, 2098 (1995).
 - ¹¹ J. C. Slater and G. F. Koster, *Phys. Rev.* **94**, 1498 (1954).
 - ¹² T. Mizokawa and A. Fujimori, *Phys. Rev. B* **51**, 12880 (1995).
 - ¹³ T. Sakudo and H. Unoki, *Phys. Rev. Lett.* **26**, 851 (1971); K. A. Müller and H. Burkard, *Phys. Rev. B* **19**, 3593 (1973).
 - ¹⁴ Y. Okimoto, T. Katsufuji, Y. Okada, T. Arima, and Y. Tokura, *Phys. Rev. B* **51**, 9581 (1995).
 - ¹⁵ S. Ishihara, T. Hatakeyama, and S. Maekawa, *Phys. Rev. B* **65** 064442 (2002).
 - ¹⁶ M. Mochizuki, *J. Phys. Soc. Jpn.* **71**, 2039 (2002).
 - ¹⁷ G. Khaliullin and S. Okamoto, *Phys. Rev. Lett.* **89**, 167201 (2002).
 - ¹⁸ T. Kiyama and M. Itoh, *Phys. Rev. Lett.* **91**, 167202 (2003).
 - ¹⁹ M. Cwik, T. Lorenz, J. Baier, R. Müller, G. Andre, F. Bouree, F. Lichtenberg, A. Freimuth, R. Schmitz, E. Müller-Hartmann, and M. Braden, *Phys. Rev. B* **68**, 060401(R) (2003).
 - ²⁰ M. Mochizuki and M. Imada, *Phys. Rev. Lett.* **91**, 167203 (2003).
 - ²¹ Actually, the crossover length is dependent on both the parameters ε and U in the following way; with increasing ε , the confinement potential due to the La layer becomes weak and the crossover length becomes longer, with increasing U the electron density at each site decreases thus the crossover length becomes longer. However, ε and U dependences are weak, and qualitative behavior does not change.
 - ²² R. D. Shannon, *Acta Crystallogr., Sect. A: Cryst. Phys., Diff., Theor. Gen. Crystallogr.* **32**, 751 (1976).